[redacted] Copy
MEMO 1-16-59E

X62-70134

NASA MEMO 1-16-59E

# NASA

# MEMORANDUM

## DESIGN AND EXPERIMENTAL INVESTIGATION OF A THREE-STAGE MULTIPLE-REENTRY TURBINE

By David G. Evans

Lewis Research Center
Cleveland, Ohio





[redacted]

NATIONAL AERONAUTICS AND SPACE ADMINISTRATION
WASHINGTON
January 1959

[redacted]

NATIONAL AERONAUTICS AND SPACE ADMINISTRATION

MEMORANDUM 1-16-59E

# DESIGN AND EXPERIMENTAL INVESTIGATION OF A THREE-STAGE MULTIPLE-REENTRY TURBINE*

By David G. Evans

## SUMMARY



The results of an experimental investigation of a three-stage multiple-reentry turbine are presented in this report. The turbine, which had a single rotor with three stages proportioned around it, was designed for the basic requirements of low weight flow and high specific work output.

The results of the experimental investigation indicated that a static efficiency of 0.622 and an equivalent specific work output of 37.5 Btu per pound had been obtained at the design point. A total-pressure loss, resulting from the flow being turned and accelerated through the turbine inlet and reentry system, accounted for approximately 7 percentage points in turbine static efficiency.

The first stage produced approximately one-half of the total turbine work output, the second stage one-third, and the third stage one-sixth; whereas the turbine was designed for an equal work division between the three stages. This was the result of a unique flow phenomenon that existed within the turbine which caused an excess pressure ratio across the first stage and a deficient pressure ratio across the third stage.

It was concluded from the results of the investigation that the turbine performance was satisfactory, but that improvements could have been made by certain refinements in the design, such as relocating two of the rotor-exit guide vanes and providing for a rotor labyrinth seal and a shorter chord rotor blade design.

Author

## INTRODUCTION

A research program currently in progress at the Lewis Research Center is concerned with the investigation of several types of high-specific-work, low-weight-flow turbines required for auxiliary power unit and turbopump drive applications.

*Title, Unclassified.

One such type of turbine under consideration is a multiple-reentry turbine. In this turbine, reentry ducts are used to direct the turbine flow between successive turbine stages located in segments around a single axial-flow-type rotor. Hence, the reentry ducting collects the flow as it is exhausted from the exit of the first stage and each intermediate stage of the turbine and directs it to the inlet of the succeeding stage.

In general, the multiple-reentry turbine appears to be well suited for the high-specific-work, low-weight-flow type of application as compared with more conventional types of multistage turbines because of (1) more reasonable rotor blade heights, (2) a lighter, less complex single disk rotor, and (3) lower rotor blade operating temperatures for a given turbine-inlet temperature.



Therefore, in view of the comparative advantages of a multiple-reentry-type turbine, an experimental investigation of one such turbine was undertaken in order to determine its performance characteristics. The subject turbine selected for the investigation was a three-stage reentry turbine of full-admission, reaction-staged design. A two-dimensional sketch in figure 1(a) illustrates the general configuration of the turbine. The flow entered the turbine at station 0 and was passed through the first-stage segment of the rotor annulus (stations 1 to 2). It was then discharged into the second-stage reentry ducting, which directed it from station 2 to the second-stage segment of the rotor annulus (station 3). In this manner the flow was staged three times across the rotor.

The investigation was conducted in two phases: (1) the design, construction, and experimental testing of one of the reentry ducts, and (2) of the turbine itself. Both phases were interdependent since a knowledge of the flow behavior within the reentry ducting was required before the turbine design could be completed. This report presents the results of both phases of the investigation. In addition, the results of measurements made of the turbine interstage flow properties were used to describe the apparent effects the reentry design had on the flow characteristics within the turbine.

## SYMBOLS

A area, sq ft

$c_p$ specific heat at constant pressure, Btu/lb-$^{\circ}$R

g acceleration due to gravity, 32.17 ft/sec$^2$

h specific enthalpy, Btu/lb

$p$ absolute pressure, lb/sq ft

$R$ gas constant, ft-lb/(lb)($^{\circ}$R)

$r$ radius, in.

$T$ temperature, $^{\circ}$R

$U$ blade speed, ft/sec

$V$ absolute gas velocity, ft/sec

$W$ relative gas velocity, ft/sec

$w$ weight flow, lb/sec

$\beta$ gas-flow angle measured from axial direction, deg

$\delta$ ratio of inlet total pressure to NASA standard sea-level pressure, $p'_0/p^*$

$\gamma$ ratio of specific heats

$\varepsilon$ function of $\gamma$, $\dfrac{\gamma^*}{\gamma} \dfrac{\left(\frac{\gamma+1}{2}\right)^{\frac{\gamma}{\gamma-1}}}{\left(\frac{\gamma^*+1}{2}\right)^{\frac{\gamma^*}{\gamma^*-1}}}$

$\eta$ static efficiency, based on shaft work output and total- to static-pressure ratio across turbine, $\dfrac{\Delta h'}{c_p T'_0 \left[1 - \left(\frac{p'_0}{p_6}\right)^{\frac{1-\gamma}{\gamma}}\right]}$

$\theta_{cr}$ squared ratio of critical velocity at turbine inlet to critical velocity at NASA standard sea-level temperature, $\left(\dfrac{V_{cr}}{V^*_{cr}}\right)^2$

$\rho$ gas density, lb/cu ft

$\tau$ torque, ft-lb

$\varphi$ flow coefficient

$\psi$ total-pressure-loss coefficient

Subscripts:

cr conditions at Mach number of unity

m mean

x axial component

Stations:

a inlet of reentry duct (fig. 1)

b inside reentry duct inside elbow

c inside reentry duct just downstream of elbow

d reentry-duct exit, normal to flow

e exit of reentry duct

0 turbine inlet

1 rotor inlet, first stage

2 rotor exit, first stage

3 rotor inlet, second stage

4 rotor exit, second stage

5 rotor inlet, third stage

6 rotor exit, third stage

7 3 feet downstream of station 6

Superscripts:

* NASA standard conditions

' absolute total state

Designations:

A first reentry duct, second-stage reentry

B second reentry duct, second-stage reentry

C first reentry duct, third-stage reentry

D second reentry duct, third-stage reentry

E third reentry duct, third-stage reentry

## TURBINE DESIGN

### Design Requirements



The turbine design-point parameters selected were:

| | |
|---|---|
| Equivalent specific work, $\Delta h'/\theta_{cr}$, Btu/lb | 45.2 |
| Equivalent weight flow, $\varepsilon w\sqrt{\theta_{cr}}/\delta$, lb/sec | 0.516 |
| Equivalent blade speed, $U_m/\sqrt{\theta_{cr}}$, ft/sec | 382.3 |

A value of static efficiency was assumed:

| | |
|---|---|
| Turbine static efficiency, $\eta$ | 0.75 |

This resulted in:

| | |
|---|---|
| Over-all total- to static-pressure ratio, $p_0'/p_6$ | 10.1 |

The assumed value of 0.75 for $\eta$ included a 7.4-percentage-point reduction in turbine static efficiency to account for total-pressure losses within the turbine ducting (Reentry-Duct Design section). Turbine work was specified to be equally divided among the three stages.

### Velocity Diagrams

Design velocity diagrams were constructed at the blade hub, mean, and tip sections to meet the requirements of free vortex flow, simple radial equilibrium, and equal flow velocities at each of the rotor inlets and exits for the three stages. The mean-blade-section velocity diagrams are shown in figure 2 for the first, second, and third stages of the turbine. The corresponding critical velocity ratios increased from stage to stage because the temperature of the flow and, hence, the critical velocity $V_{cr}$ dropped. The small variation in the velocity diagram values of $\beta_{1,3,5}$ and $\beta_{2,4,6}$ just inside the ducting of each of the three stages was not incorporated in the turbine. Average values of $68.2^\circ$ and $35.8^\circ$, respectively, were used.

The velocity diagrams just inside the rotor trailing edge and inside the ducting inlets and exits were constructed from the corresponding free-stream velocity diagrams by assuming (1) no change in the tangential component of velocity and (2) continuity with no loss in total pressure in going from the free-stream conditions. The blockage just inside the ducting resulted from a guide vane located at the discharge end of the turbine-inlet duct and at each end of the reentry ducting. One turbine-inlet duct and five reentry ducts were used in the turbine design, hence the blockage resulted from six guide vanes, each 3/16 inch thick. The blockage just inside the trailing edge of the rotor was calculated for 126 blades having a trailing-edge thickness of 0.010 inch.



## Rotor Design

The turbine rotor was designed for the specification of zero suction-surface diffusion and the assumption of simple radial equilibrium. The design involved an iterative process where the rotor hub, mean, and tip sections were laid out in the manner described in reference 1 and analyzed by the method of reference 2. The layouts were then altered and reanalyzed until continuity and the condition of zero suction-surface diffusion had been obtained.

Satisfying the above specifications resulted in a rotor design of 126 blades with an axial chord of 0.640 inch and a blade solidity, defined as the ratio of the blade chord to blade pitch, of 2.42 at the hub section and 2.26 at the tip section. The resulting blade profiles are shown in figure 3 along with the blade surface and midchannel velocity distributions between the first and last channel orthogonals. Blade coordinates and orientation angles are given in table I along with the radial-axial coordinates of the rotor blade inner and outer walls.

## Reentry-Duct Design

The reentry ducting as well as the turbine-inlet duct was designed to turn and accelerate the flow directly into the rotor. Although a better flow distribution might have been obtained at the rotor inlet by using a conventional stator section upstream of the rotor, it was felt that the over-all turbine performance would be improved by eliminating the stator section with its associated losses in total pressure. Furthermore, this design allowed all the available acceleration of the flow to be taken within the ducting, which minimized the amount of diffusion, separation, and boundary-layer growth in the turns and along the walls.

A variation in the cross-sectional area of the reentry ducting was proportioned to smoothly accelerate the flow along the length of the ducting.

A study of various reentry-duct configurations was made, and selection of the final design was governed by the following considerations:

(1) Imparting of the least amount of distortion and loss in total pressure to the flow

(2) Minimum increase in the over-all size of the turbine

(3) Feasibility of construction.



The resulting configuration shown in figures 4(a) and (b) employed one inlet duct, two second-stage reentry ducts, and three third-stage reentry ducts. By proportioning the flow in this manner among several reentry ducts, the volume rate of flow and, hence, the cross-sectional area of each duct were approximately equal. In so doing, the over-all size of the turbine was minimized. The reentry ducts were lettered A to E as noted in the figure.

In order to establish the design turbine static efficiency and total- to static-pressure ratio, some knowledge was required of the magnitude of the total-pressure losses within the reentry ducting. Therefore, a test model of a reentry duct was built and tested to determine its flow characteristics. A description of this test is given in the section entitled Reentry-Duct Test. The design requirements of the test duct were:

| | |
|---|---|
| Duct-inlet critical velocity ratio, $(V/V_{cr})_a$ | 0.385 |
| Duct-exit critical velocity ratio, $(V/V_{cr})_e$ | 0.926 |
| Duct-inlet angle, $\beta_a$, deg | 38.7 |
| Duct-exit angle, $\beta_e$, deg | 70.0 |

The station nomenclature for the test duct is given in figure 1(b). The over-all dimensions of the test duct were selected to approximate those of reentry duct C because duct C represented average dimensions of size, length, and turning. The final dimensions of reentry duct C as well as the other reentry ducts were then based on the performance of the test duct. The test duct is shown in its test facility in figure 5.

The results of the experimental investigation of the test duct are presented in figure 6(a) in terms of the critical velocity ratio $V/V_{cr}$ of the flow in the duct to a total-pressure-loss coefficient $\psi$ where

$$\psi_{a-e} \equiv \frac{p'_a - p'_e}{p'_a} = 1 - \frac{p'_e}{p'_a}$$

Instrumentation located at stations a to e was used to compute the variation of the total-pressure-loss coefficient $\psi$ and the critical velocity ratio $V/V_{cr}$ along the length of the duct. Calculations were made using the continuity relations, the measured values of static pressure at each station, the total temperature, and the weight flow entering the duct. The experimentally obtained value of $\psi_{a-e}$ was 0.10. This corresponded to an acceleration of the flow from a critical velocity ratio of 0.32 at the duct inlet (station a) to 0.91 at the duct exit (station e). In two subsequent runs, numbers 2 and 3 in figure 6(a), the effect of reducing the velocity level in the duct did not substantially change the measured values of $\psi$ from station to station.

Figure 6(b) presents the results of a total-pressure survey made at the exit of the test duct (station e) for run number 1. Areas of large boundary-layer buildup and possible flow separation are noted along the walls, particularly around the area on the left side of the figure. Survey results are not shown for runs 2 and 3 because there was no substantial change in the profiles. The surveys were used, however, to obtain area-averaged and momentum-averaged values of the exit total pressure $p'_e$ as a check against the values computed from the continuity relations. The values checked with those based on continuity within 2 percent.

Based on the results of the reentry-duct test, an over-all second-stage reentry loss coefficient $\psi_{2-3}$ of 0.10 and a third-stage $\psi_{4-5}$ of 0.11 were used. An inlet duct $\psi_{0-1}$ of 0.06 was used. The effect of this loss in flow total pressure on the turbine over-all static efficiency was computed as 7.4 percentage points. This effect was therefore taken into account in establishing the turbine stage area ratios.

## Final Turbine Geometry

The reentry turbine investigated was a 12.6-inch (tip diameter) cold-air turbine having a rotor-inlet hub-tip radius ratio of 0.865 and an exit hub-tip radius ratio of 0.825. The turbine is shown diagrammatically in figure 7. Photographs are presented in figure 8. Inlet arcs of admission for the three stages were $58.8^\circ$, $103.1^\circ$, and $198.1^\circ$.

The first-stage exit guide vane, shown in figure 7 (section A-A), was offset relative to the inlet guide vane such that the flow leaving the inlet guide vane would impinge on the exit vane, exactly dividing the first- and third-stage flows. This relative offset between guide vanes, noted in the figure, was $7.9^\circ$. The offset between the vanes of the first- and second- and the second- and third-stage flows, however, was set at $4.7^\circ$ and $2.3^\circ$, respectively. This was done to satisfy the given design condition of equal work split and equal blade height per stage, which

required the area ratios across each stage to increase slightly from the first to third stages. Therefore, the exit arc of each stage of the turbine was proportioned to give the required area ratio.

A radial clearance of 0.020 inch was used between the tip of the rotor blading and the turbine casing. Axial clearances between the rotor blading and guide vanes and between the turbine inner fairings and rotor were 0.015 inch. These clearances are noted in the insert in figure 7.



## EXPERIMENTAL PROGRAM

### Reentry-Duct Test



Description of apparatus. - A photograph of the test facility used to investigate the flow behavior within the reentry test duct is shown in figure 5. The facility consisted primarily of the reentry-duct test model, a bellmouth-shaped adapter to give uniform flow conditions into the duct, and a survey probe actuator. Pressurized air from the laboratory combustion air supply was directed through a hydraulically operated inlet control valve, an ASME thin-plate orifice, and a screen to the bellmouth adapter. The flow exhausted directly into the room. The material used to fabricate the reentry duct and the bellmouth adapter was fiber glass.

Instrumentation. - The inlet total-temperature and total-pressure measurements for the reentry-duct test were made upstream of the bellmouth adapter. Variations in flow static pressure were obtained at four stations along the length of the reentry duct with four wall static taps located at each station. Static pressure at the exit of the reentry duct was assumed to equal the barometric pressure since the flow discharged directly into the room. In addition, detailed circumferential and radial total-pressure surveys were made at the exit with a fixed-angle total-pressure probe mounted on an actuator. The total-pressure variation was plotted against probe travel on an X-Y recording potentiometer.

All pressure measurements were made with mercury manometers, except for the pressure differential across the orifice, which was measured with an acetylene tetrabromide manometer.

Test procedure. - The reentry test duct facility was operated at a constant temperature of 540° R at three inlet total pressures of 56.0, 51.5, and 47.0 inches of mercury absolute, designated as runs 1, 2, and 3, respectively (fig. 6(a)). It was felt that this range of inlet total pressures sufficiently covered the design point in addition to obtaining the effect of reducing the velocity level in the duct on the total-pressure-loss coefficient $\psi$. At each setting pressure, a detailed circumferential and radial survey of total pressure was made at the duct

exit (station e). From the surveys, area-averaged and momentum-averaged values of the exit total pressure $p'_e$ were obtained, in addition to a general perspective of the flow profile leaving the duct.

## Turbine Test

Description of apparatus. - The turbine test facility was operated on dry pressurized air from the laboratory combustion air system. Before entering the turbine-inlet duct, the air was passed through a filtering tank, a steam heat exchanger, an electric heater, a hydraulically operated inlet control valve, a calibrated ASME thin-plate orifice, and a screen. The air was exhausted from the turbine through a hydraulically operated exit control valve to the laboratory altitude exhaust system. The power output of the turbine was absorbed by a cradle-mounted direct-current dynamometer.

The rotor blades and wheel were machined from SAE 4340 steel, and the blades pinned in the wheel with steel roll pins. The turbine-inlet duct and five reentry ducts were formed of pure nickel by the process of electroforming. The interior walls of the ducting had a surface finish of approximately 8 microinches and a dimensional accuracy of 0.002 inch. The process of electroforming is explained more fully in reference 3.

Instrumentation. - The turbine-inlet temperature was measured by averaging the readings of two bare-wire thermocouples at station 0. Inlet total pressure was also obtained at station 0 by averaging the readings of three total-pressure probes. Turbine-exit static pressure at station 6 was obtained by averaging the readings of 15 equally spaced wall static taps located around the inner and outer annulus walls. Also at station 6, exit total pressure, total temperature, and absolute flow angle were measured at a mean radial position at three equally spaced points around the exit annulus with three combination probes mounted on self-alining actuators. The turbine output torque was measured with a commercial self-balancing torque cell connected to a mercury manometer. Turbine rotative speed was measured with an electronic events-per-unit-time meter.

In addition to the instrumentation at the turbine inlet and exit, instrumentation was placed within the reentry ducting to evaluate stage performance. The total temperatures, total pressures, and static pressures were measured at station c (fig. 1(b)) in each of the reentry ducts. To accomplish this, several wall static taps and a combination rake of one thermocouple and two total-pressure probes were installed. A rake of six total-pressure probes was also located at the mean radius of the exit guide vane separating the first and third stages. This rake is noted in section A-A of figure 7.

All pressure measurements were made with mercury manometers, except for the pressure upstream of the orifice, which was measured with a calibrated Bourdon-type gage.

Test procedure. - The turbine facility was operated at a constant inlet pressure (station 0) of 110 inches of mercury absolute and a constant inlet temperature of 740° R. Performance runs were made at speeds of from 0 to 100 percent design speed, and the turbine total- to static-pressure ratio varied from approximately 4 to as high as 30 for each speed.





## EXPERIMENTAL RESULTS

### Over-All Turbine Performance

Over-all turbine performance is presented in figure 9. In figures 9(a) and (b), the equivalent specific work output $\Delta h'/\theta_{cr}$ and static efficiency $\eta$ are shown as a function of the total- to static-pressure ratio over the range of speeds investigated. At design conditions, an equivalent specific work output of 37.5 Btu per pound was obtained at a static efficiency of 0.622. It can be seen in figure 9(a) that a significant increase in turbine equivalent specific work was obtained between the design total- to static-pressure ratio of 10.1 and the limiting-loading total- to static-pressure ratio of approximately 30. At design speed, the limiting-loading equivalent specific work output was 42.6 Btu per pound, which was approximately 6 percent below the design equivalent specific work of 45.2 Btu per pound. The maximum static efficiency was 64 percent, which was obtained at design speed and a total- to static-pressure ratio of 6.

In figure 9(c) the variation of equivalent torque $\tau/\delta\varepsilon$ with percent design speed is shown for the design total- to static-pressure ratio of 10.1. The ratio between zero-speed (starting) equivalent torque and design-speed equivalent torque was 1.8.

The measured turbine equivalent weight flow was approximately 3 percent greater than design. This was due to an overexpansion of the flow across the first stage of the turbine, which caused the turbine-inlet duct to choke. This overexpansion increased the critical velocity ratio at station 1 from its design value of 0.815 to 1.00, which increased the equivalent weight flow from 0.516 to 0.532 pound per second.

### Interstage Characteristics

Total temperature, total pressure, and static pressure were measured at the turbine inlet and exit and within each of the reentry ducts. They were then expressed as a ratio of their corresponding total state

condition at the turbine inlet and are presented in figures 10(a), (b), and (c) for design speed and design total- to static-pressure ratio. Approximately one-half of the total-temperature drop across the turbine was taken across the first stage, whereas the drop across the second and third stages was approximately one-third and one-sixth, respectively, of the total-temperature drop (fig. 10(a)). The temperature measurements are presented herein as only an approximate indication of the turbine stage performance. The over-all turbine work output based on torque measurements checked within 5 percent of the work output based on temperature measurements.



It may be noted that the turbine rotor blading was exposed to the inlet flow temperature over only a fraction of each revolution. The inlet arc covered one-sixth of the turbine annulus, whereas the lower temperature second and third stages covered approximately one-third and one-half of the turbine annulus, respectively. The rotor blading was therefore operating at a temperature somewhere between the temperatures of the second- and third-stage flows.

Figures 10(b) and (c) show the variation of total and static pressures within the turbine, expressed as a ratio of the turbine-inlet total pressure. The points indicated as experimental data were actual values measured at the turbine inlet and exit and within the five reentry ducts at a station corresponding to station c in the reentry test duct. The points indicated as extrapolated data were obtained by assuming the same variation in total pressure along the length of the reentry ducting as was obtained in the reentry-duct test. The dashed lines on the figures indicate the design variation of static and total pressures.

A comparison of the experimentally obtained pressures with the design pressures in figure 10(b) and (c) indicated that both the static and total pressures between the turbine inlet and exit were below design. It was observed from the results in figure 10(b) that the flow overexpanded across the first stage and underexpanded across the third stage. The second-stage total-pressure ratio was approximately equal to design. The apparent cause of the total-pressure-ratio deviation from design will be discussed in the ANALYSIS OF RESULTS section. This deviation increased the first-stage specific work output from one-third to approximately one-half of the total specific work output while similarly reducing the third-stage specific work output from one-third to approximately one-sixth of the total specific work output.

## ANALYSIS OF RESULTS

From the values of total-pressure, static-pressure, and total-temperature measurements in the five reentry ducts at the stations

corresponding to station c in the test duct, the weight flows were computed by using the following relation:

$$w = \left(\frac{\rho V}{\rho' V_{cr}}\right)(\rho' V_{cr})(\varphi A)$$

or

$$w = \left(\frac{\rho V}{\rho' V_{cr}}\right)\left(\frac{p'}{\sqrt{T'}}\right)\sqrt{\frac{2\gamma g}{(\gamma + 1)R}}\,(\varphi A)$$

A value for $\varphi$ (an assumed flow coefficient to compensate for wall boundary layer) of 0.98 was used. The values for the weight-flow parameter $\rho V/\rho' V_{cr}$ were obtained from the relation:

$$\frac{\rho V}{\rho' V_{cr}} = \left\{\frac{\gamma + 1}{\gamma - 1}\left[\left(\frac{p}{p'}\right)^{2/\gamma} - \left(\frac{p}{p'}\right)^{\frac{\gamma+1}{\gamma}}\right]\right\}^{1/2}$$

Results of the calculations are given in a bar graph comparison of the reentry weight flows (fig. 10(d)). Approximately 82 percent of the turbine-inlet flow entered the second-stage reentry ducting (ducts A and B), and 84 percent entered the third-stage reentry ducting (ducts C, D, and E).

Although the interstage flow characteristics can be considered only an approximate indication of the flow conditions within the turbine, they were used to analyze the general flow phenomena that existed within the turbine. The interstage weight flow calculations indicated a deficiency in the weight flow within the reentry ducting in comparison with the weight flow entering the turbine. Between the first and second stages there was a deficiency of approximately 18 percent, and between the second and third stages there was a deficiency of approximately 16 percent.

There were three general areas within the turbine where it was believed an interstage transport of flow could occur, other than through the reentry system. They were (1) displacement of flow from within each stage caused by the rotor carrying the fluid within the blade passages to an adjacent stage, (2) leakage of flow from one stage to another through the clearance spaces between the rotor wheel and inner fairings and between the blade row and guide vanes, and (3) spillage of flow at the rotor exit into the wrong ducting due to the location of the exit guide vanes separating the stages. The apparent motivation for the leakage flow was the static-pressure gradient which existed around the turbine annulus. With respect to spillage flow, instrumentation located on the exit guide

vane between the first and third stages indicated that the guide vane was exactly separating the first- and third-stage flows with no apparent spillage at design turbine speed and design total- to static-pressure ratio. However, the guide vanes separating the first and second and the second and third stages were not offset by the same amount. Therefore, it is reasonable to expect that spillage may have occurred between these stages in the areas between stations 1 and 4 and stations 3 and 6 (fig. 1(a)).



The effect of the displacement, leakage, and spillage flows was apparent on the amount of flow available for doing work in each stage, but it also had the effect of changing the effective area ratios and hence the total- and static-pressure ratios across each stage. In the turbine design, the stage inlet to exit area ratios had been computed by assuming 100-percent weight flow at all stations. In the first stage, the effect of losing approximately 18 percent of the flow across the rotor increased the effective stage area ratio and hence the total- and static-pressure ratios to above their design value. In the second stage, the weight flow entering and leaving the rotor was approximately equal; therefore, the effective area ratio and total- and static-pressure ratios across the stage were approximately equal to design. Finally, the effect of an increase in weight flow across the third-stage segment of the rotor of approximately 16 percent reduced the effective area ratio and, hence, reduced the total- and static-pressure ratios across the stage to below design.

The adverse effect that the displacement, leakage, and spillage flow had on the stage performance and over-all performance of the turbine could have been reduced, possibly, by giving more attention to the design details in the areas where these flows occurred. It was felt that these flows could have been reduced by using a shorter chord rotor blade design, placing a labyrinth seal between the rotor and inner fairings, and relocating the exit guide vanes separating the first- and second- and second- and third-stage rotor-exit flows.

## SUMMARY OF RESULTS

A three-stage multiple-reentry turbine was designed and experimentally investigated. The results of the investigation are summarized as follows:

1. Over-all turbine performance results indicated that a turbine equivalent specific work output of 37.5 Btu per pound and a static efficiency of 0.622 were obtained at design speed and design total- to static-pressure ratio. At limiting loading, the equivalent specific work output was 42.6 Btu per pound, which was approximately 6 percent below the design value of 45.2 Btu per pound. Based on these results it is felt that the turbine performance is aerodynamically satisfactory.

2. Results of turbine interstage measurements indicated that, at design speed and design total- to static-pressure ratio, approximately one-half of the turbine work was done by the first stage, one-third by the second stage, and the remaining one-sixth by the third stage, compared with the design requirement of equal work split per stage. This unbalanced division of work appeared to have resulted from the effect that the displacement, leakage, and spillage flows had on the stage weight flows. This in turn brought about a change in the effective stage area ratios and pressure ratios and, hence, the stage work outputs.

3. Results of the reentry-duct investigation indicated that the total-pressure losses due to turning and accelerating the flow through the turbine inlet and reentry system accounted for approximately 7 percentage points in turbine over-all static efficiency.

Lewis Research Center
National Aeronautics and Space Administration
Cleveland, Ohio, October 20, 1958

## REFERENCES

1. Stewart, Warner L., Wong, Robert Y., and Evans, David G.: Design and Experimental Investigation of Transonic Turbine with Slight Negative Reaction Across Rotor Hub. NACA RM E53L29a, 1954.

2. Whitney, Warren J., Monroe, Daniel E., and Wong, Robert Y.: Investigation of Transonic Turbine Designed for Zero Diffusion of Suction-Surface Velocity. NACA RM E54F23, 1954.

3. Lamb, Vernon A., and Metzger, Wm. H., Jr.: Electroforming - A Method for Producing Intricate Shapes. IM 10-54-2975, The International Nickel Co., Inc., 1954. (See also The Tool Engineer, vol. 33, Aug. 1954, pp. 55-62.)

[redacted]

TABLE I. - ROTOR-BLADE-SECTION AND WALL CONTOUR COORDINATES

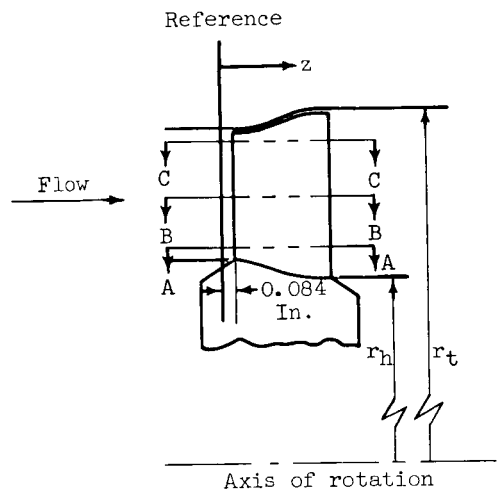


| Reference | z, in. | $r_h$, in. | $r_t$, in. |
|---|---|---|---|
| | 0 | 5.350 | 6.180 |
| | .084 | 5.347 | 6.183 |
| | .100 | 5.345 | 6.185 |
| | .150 | 5.335 | 6.195 |
| | .200 | 5.320 | 6.210 |
| | .250 | 5.302 | 6.227 |
| | .300 | 5.280 | 6.249 |
| | .350 | 5.260 | 6.267 |
| | .400 | 5.246 | 6.284 |
| | .450 | 5.234 | 6.295 |
| | .500 | 5.225 | 6.305 |
| | .550 | 5.220 | 6.310 |
| | .600 | 5.215 | 6.315 |
| | .650 | 5.212 | 6.317 |
| | .700 | 5.210 | 6.319 |
| | .724 | 5.210 | 6.320 |

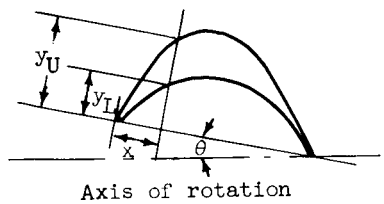


| | Section | | | | | |
|---|---|---|---|---|---|---|
| | A-A | | B-B | | C-C | |
| | r, in. | | | | | |
| | 5.405 | | 5.765 | | 6.125 | |
| | $\theta$ | | | | | |
| | $12^\circ32'$ | | $15^\circ45'$ | | $22^\circ30'$ | |
| x, in. | $y_L$, in. | $y_U$, in. | $y_L$, in. | $y_U$, in. | $y_L$, in. | $y_U$, in. |
| 0 | 0.004 | 0.004 | 0.005 | 0.005 | 0.006 | 0.006 |
| .05 | .068 | .149 | .067 | .142 | .053 | .151 |
| .10 | .123 | .250 | .121 | .239 | .098 | .230 |
| .15 | .161 | .309 | .156 | .290 | .130 | .271 |
| .20 | .186 | .340 | .180 | .316 | .153 | .292 |
| .25 | .201 | .352 | .196 | .326 | .168 | .299 |
| .30 | .209 | .349 | .204 | .324 | .176 | .294 |
| .35 | .208 | .332 | .204 | .309 | .178 | .279 |
| .40 | .199 | .299 | .196 | .281 | .172 | .253 |
| .45 | .181 | .254 | .180 | .240 | .159 | .219 |
| .50 | .152 | .197 | .153 | .188 | .138 | .178 |
| .55 | .111 | .136 | .112 | .133 | .110 | .133 |
| .60 | .057 | .075 | .062 | .077 | .073 | .089 |
| .65 | .000 | .014 | .008 | .022 | .031 | .045 |
| .655 | .005 | .005 | ---- | ---- | ---- | ---- |
| .664 | ---- | ---- | .005 | .005 | ---- | ---- |
| .675 | ---- | ---- | ---- | ---- | .008 | .022 |
| .692 | ---- | ---- | ---- | ---- | .005 | .005 |

[redacted]

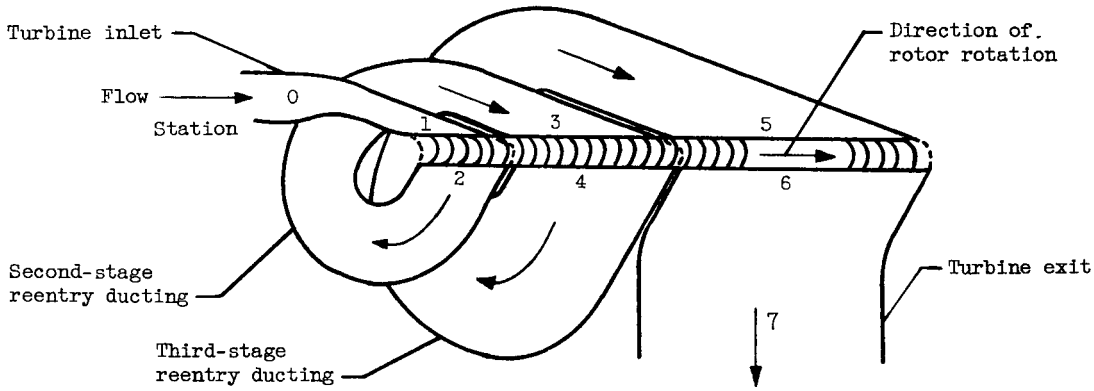


(a) Turbine two-dimensional layout.

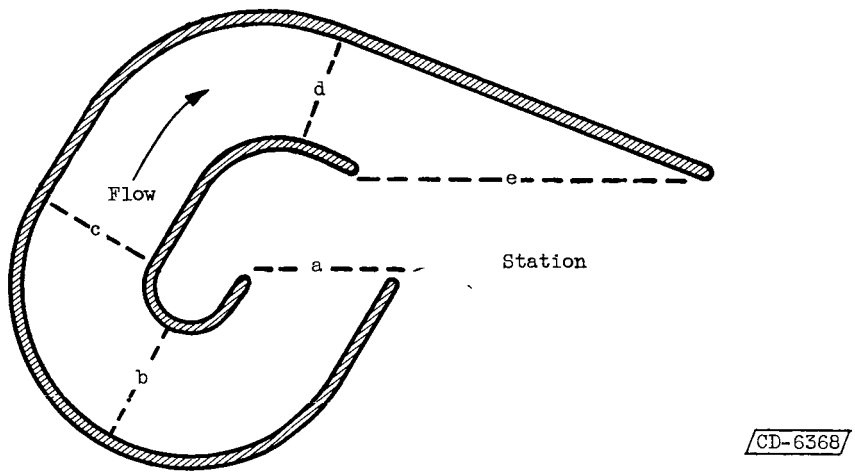


(b) Reentry test duct.

Figure 1. - Diagrammatic sketches of reentry turbine and test duct.

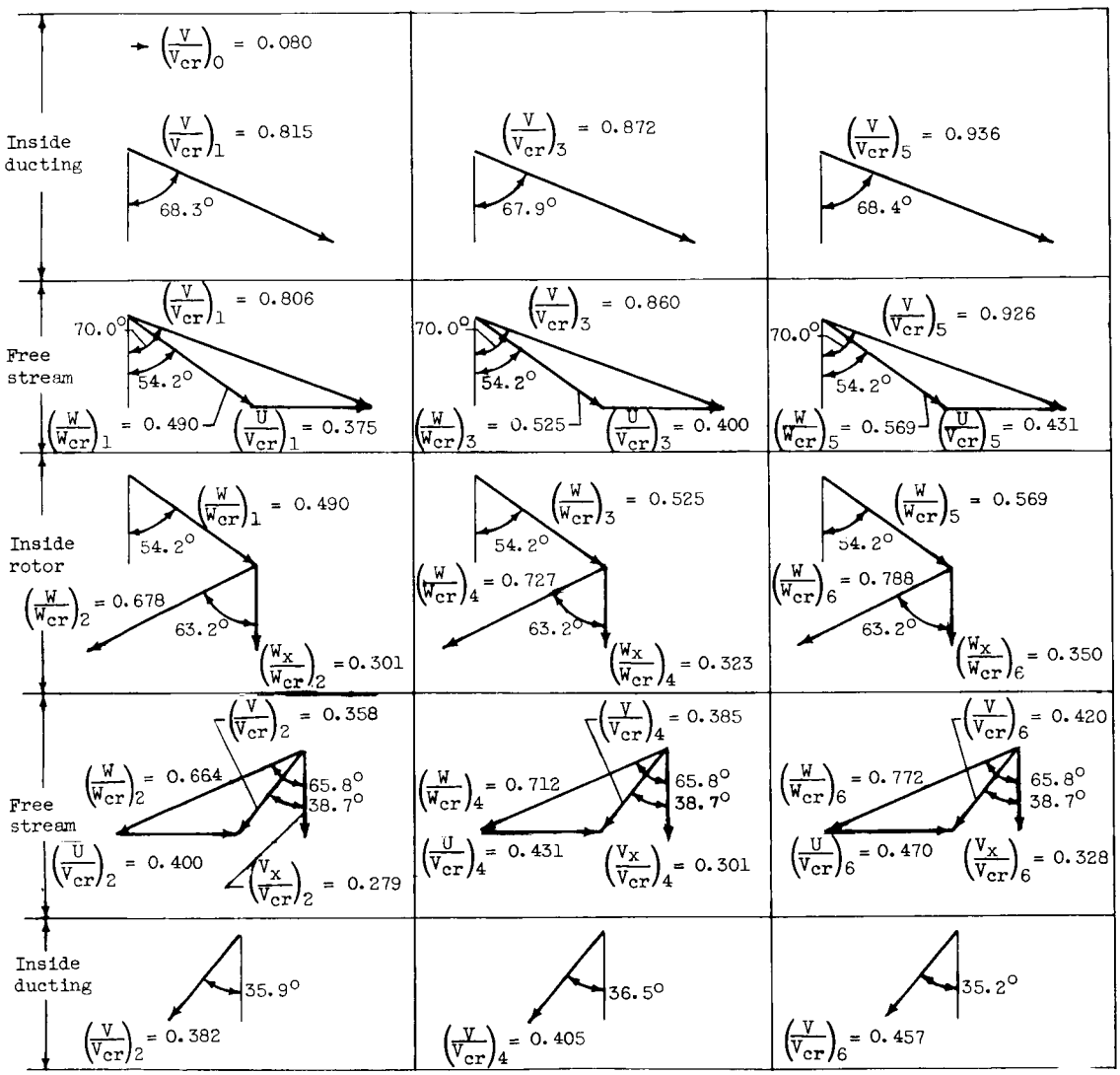


(a) First stage. (b) Second stage. (c) Third stage.

Figure 2. - Reentry turbine mean-blade-section velocity diagrams. Radius, 5.765 inches.

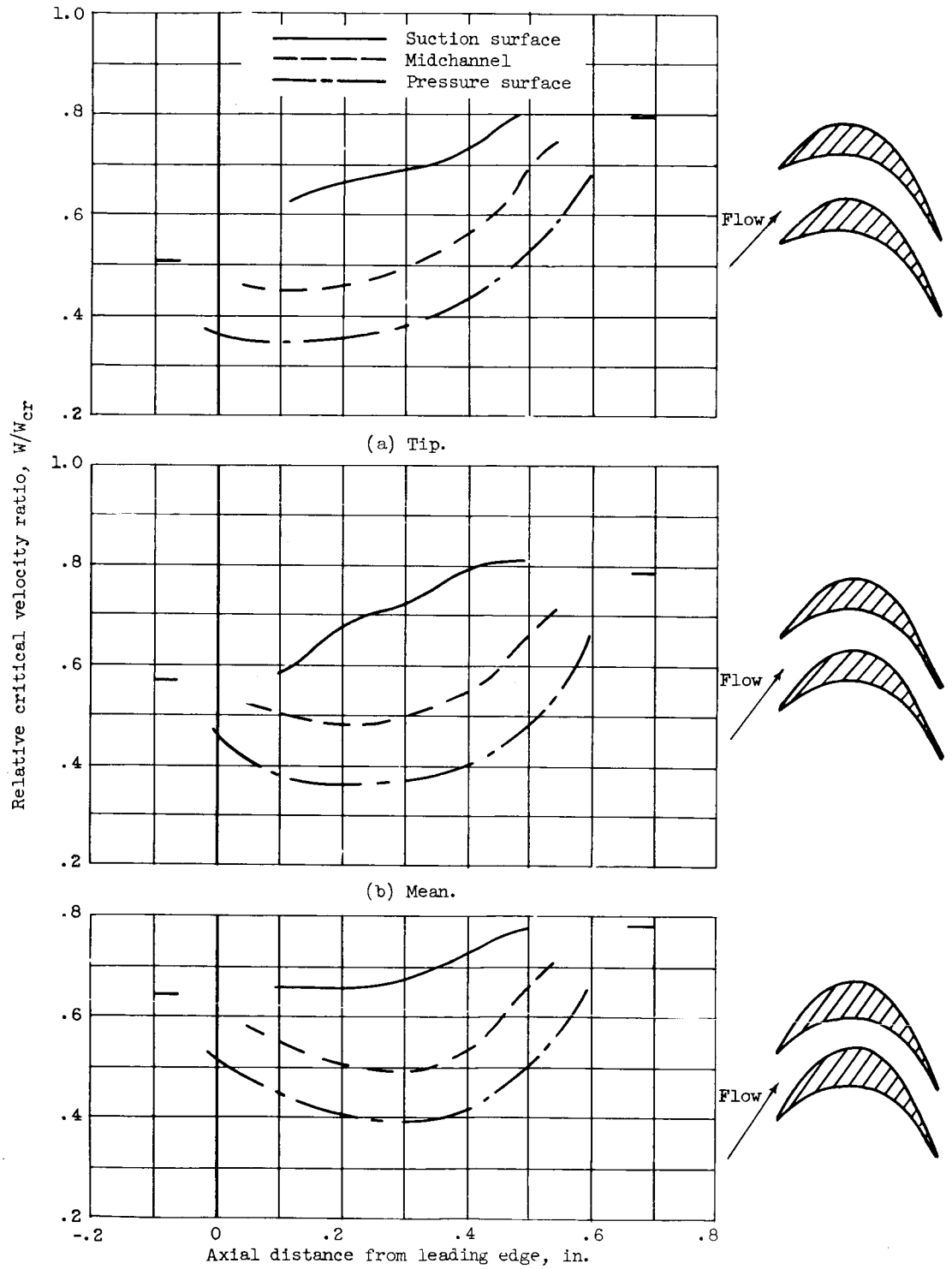


(a) Tip.

(b) Mean.

(c) Hub.

Figure 3. - Blade profiles and third-stage design blade velocity distributions.

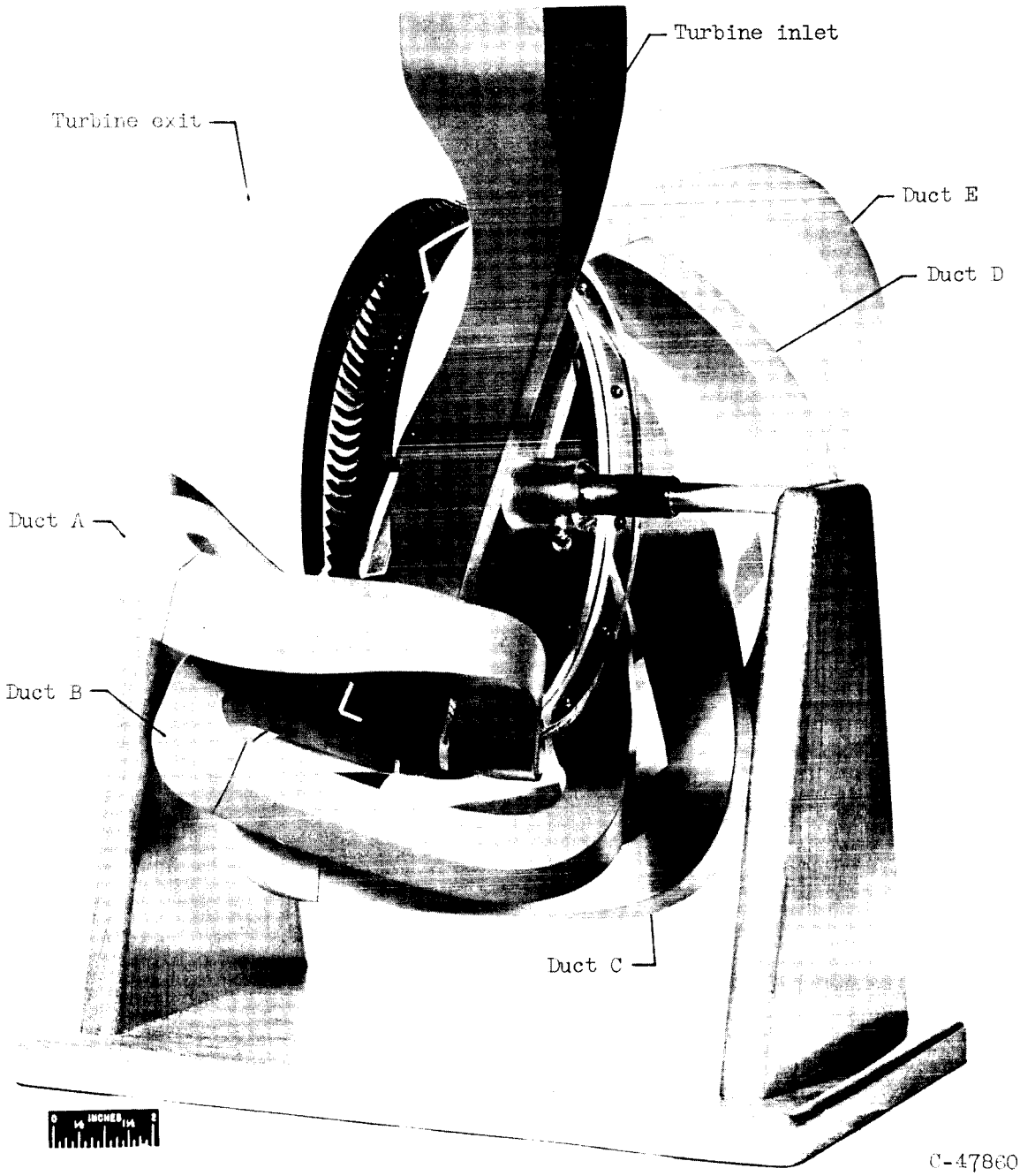


(a) Front of turbine.

Figure 4. - Three-dimensional mockup of turbine assembly.

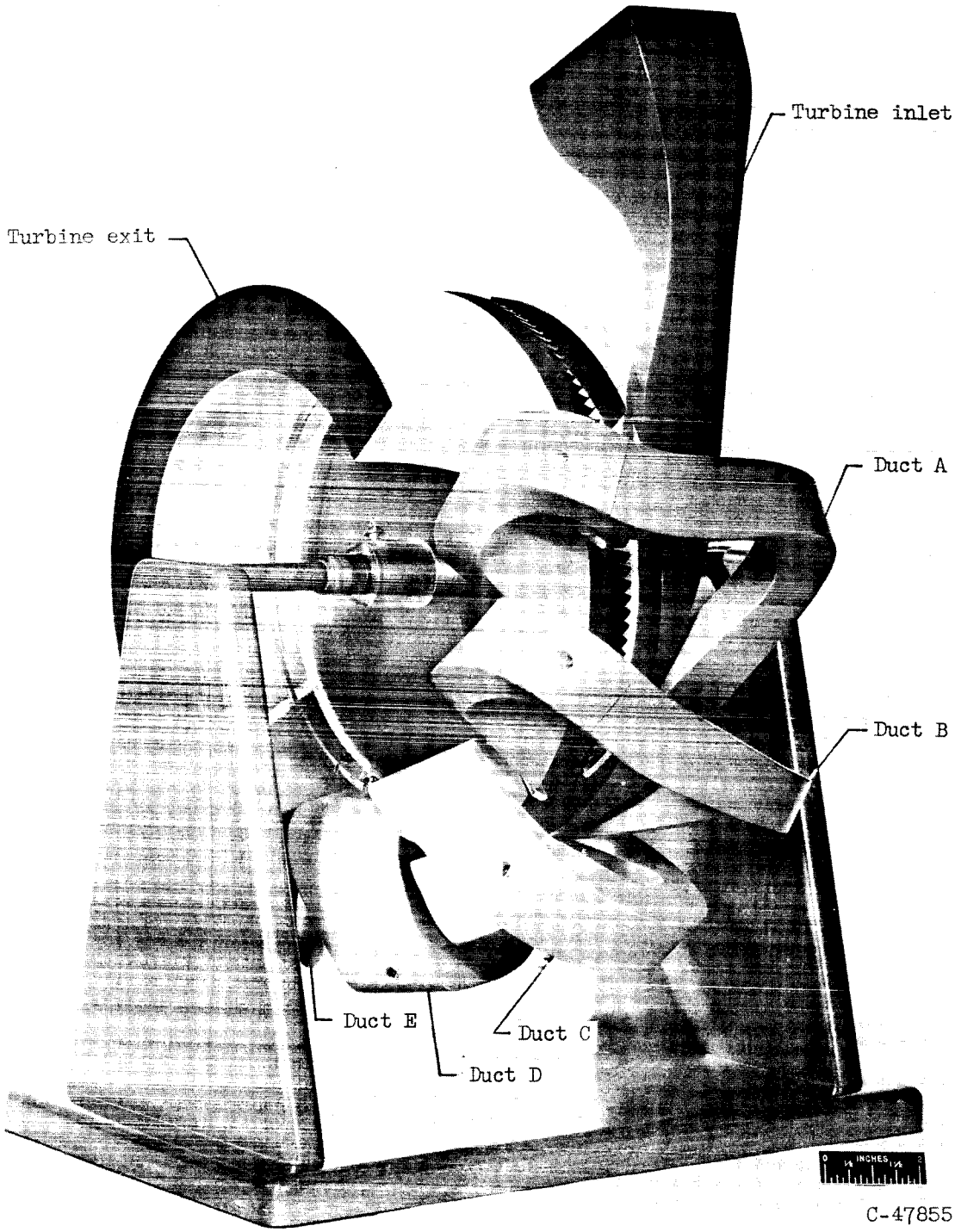


(b) Back of turbine.

Figure 4. - Concluded. Three-dimensional mockup of turbine assembly.

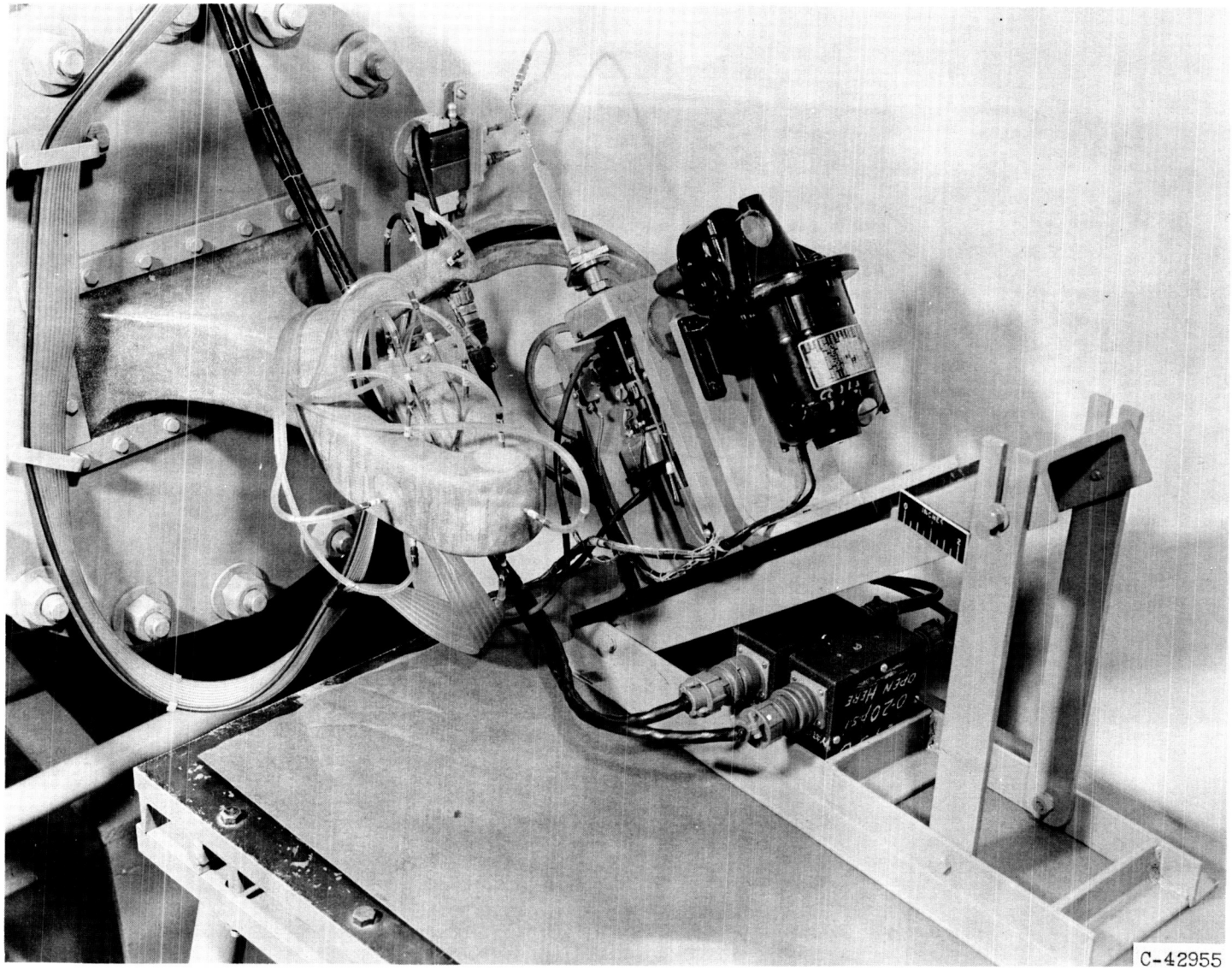


Figure 5. - Reentry-duct test facility.

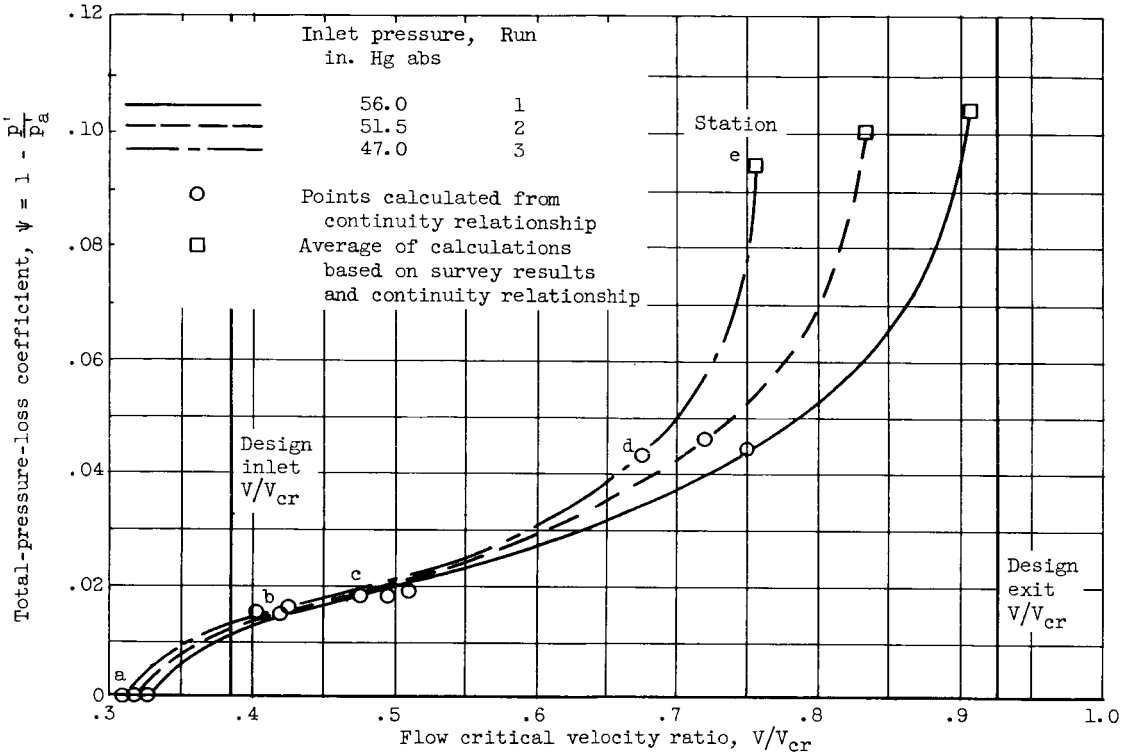


(a) Variation of total-pressure-loss coefficient and critical velocity ratio within reentry duct for three inlet pressures.

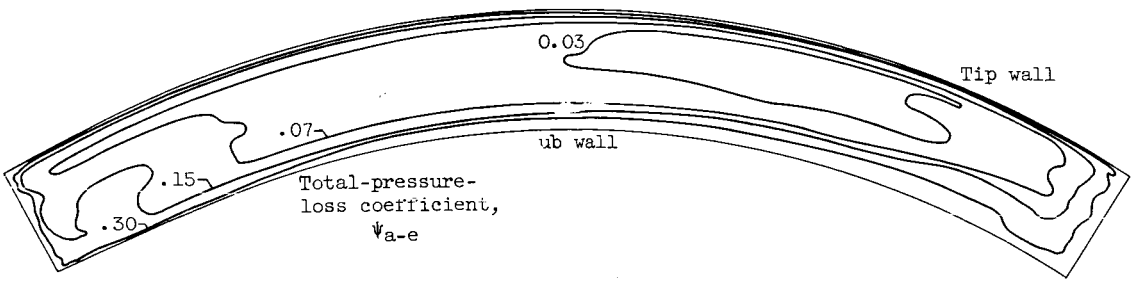


(b) Contours of total-pressure-loss coefficient at station e at an exit critical velocity ratio of 0.91.

Figure 6. - Experimental performance results of reentry test duct.

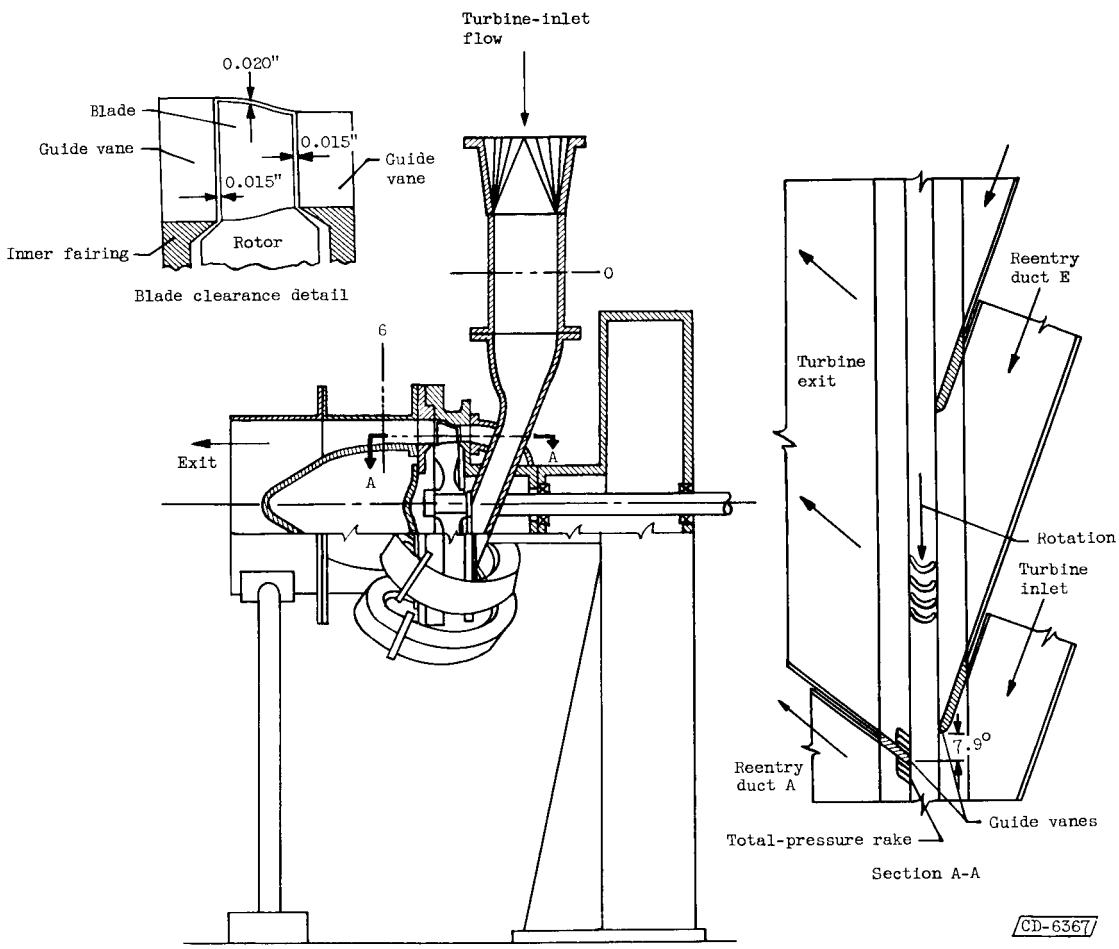


Figure 7. - Diagrammatic sketch of reentry turbine test section.

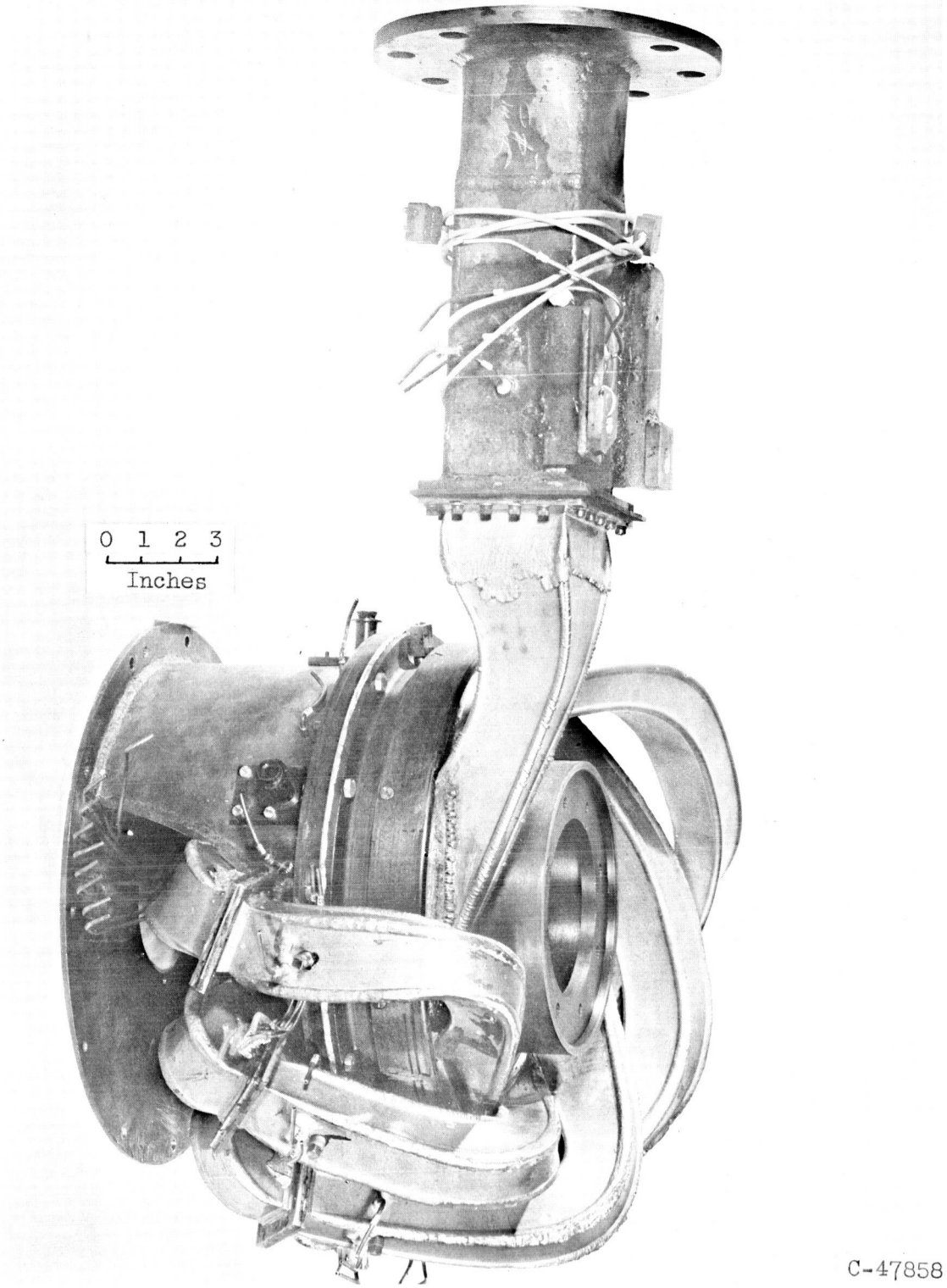


(a) Turbine assembly with inlet, reentry, and exit ducting in place.

Figure 8. - Photographs of reentry turbine.

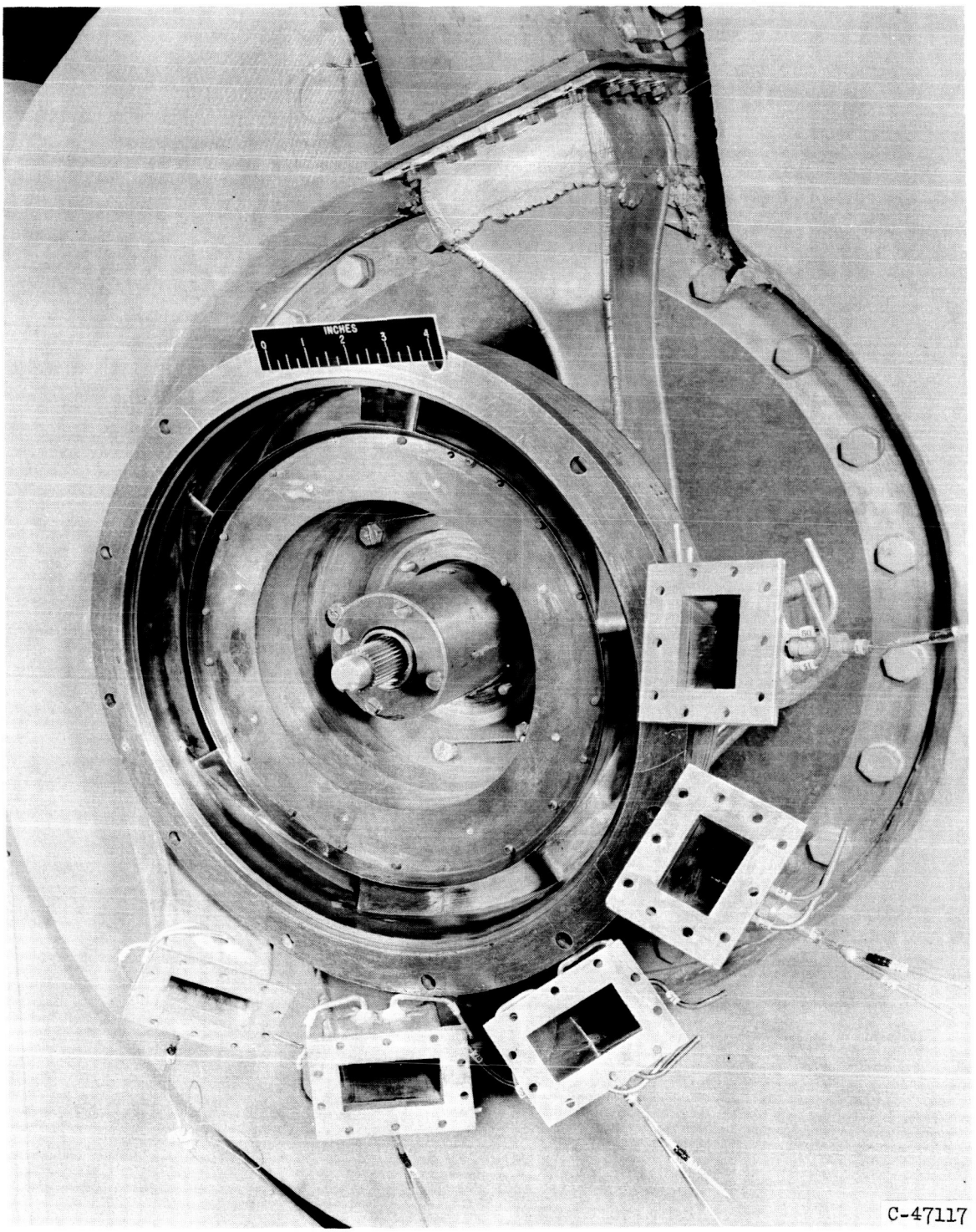


(b) Front half of turbine mounted on test facility.

Figure 8. - Continued. Photographs of reentry turbine.

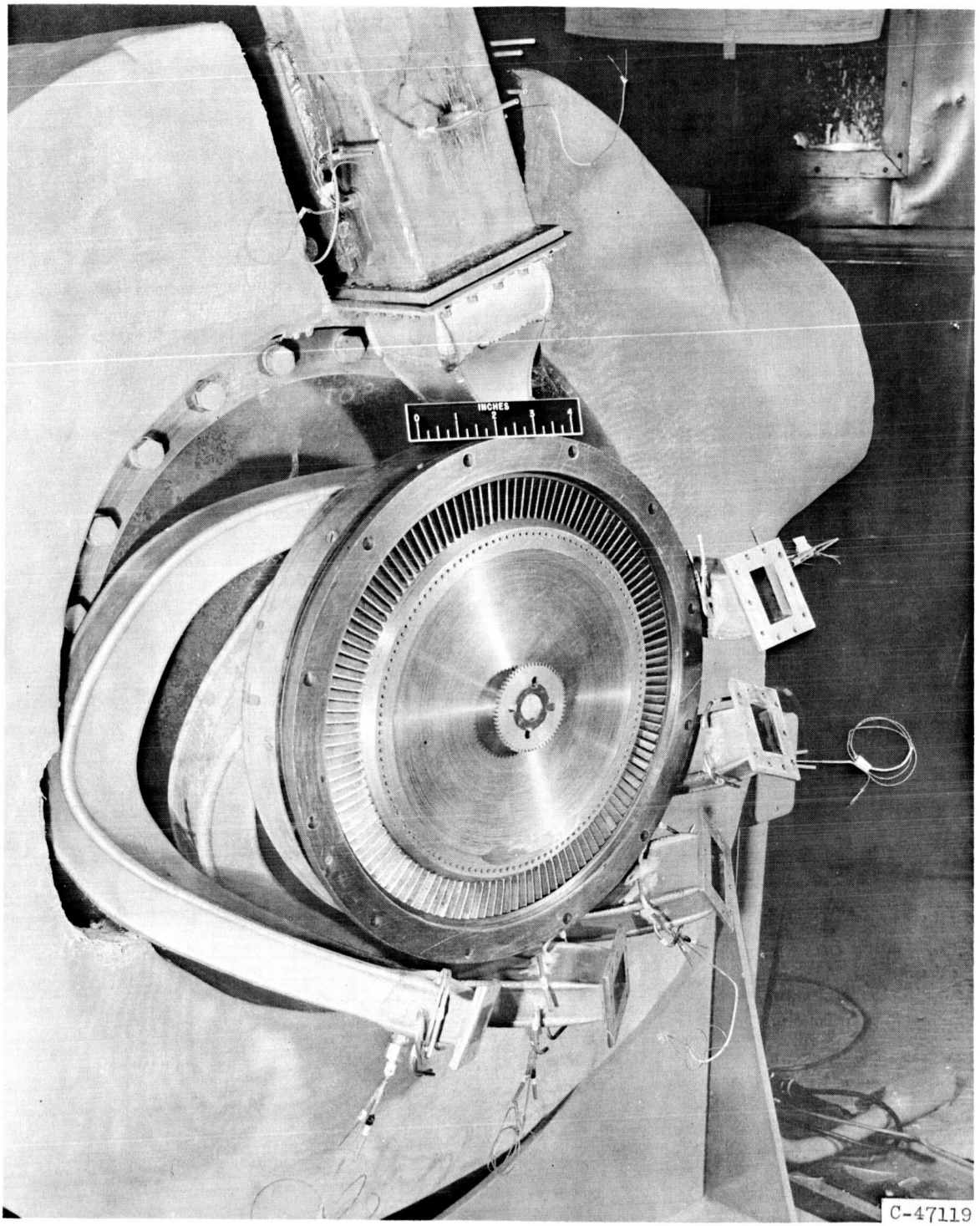


(c) Front half of turbine and rotor mounted on test facility.

Figure 8. - Concluded. Photographs of reentry turbine.

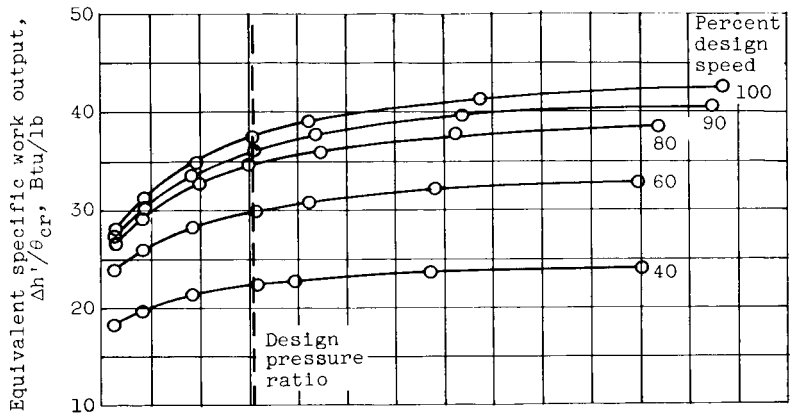


(a) Variation of work output with total- to static-pressure ratio over range of speeds.

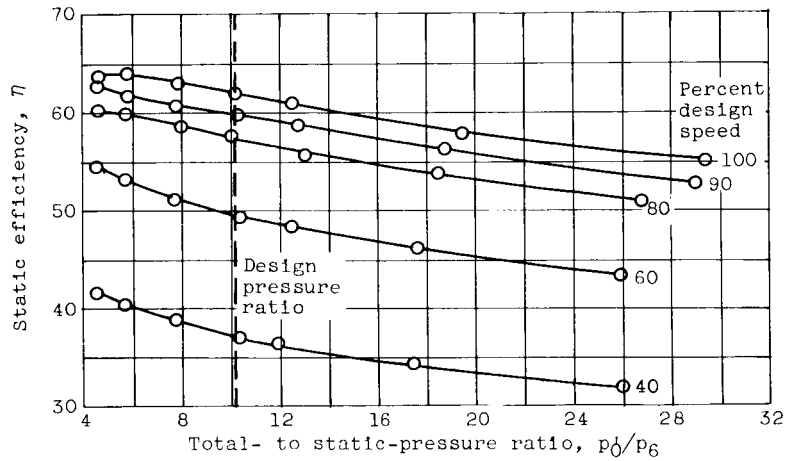


(b) Variation of static efficiency with total- to static-pressure ratio over range of speeds.

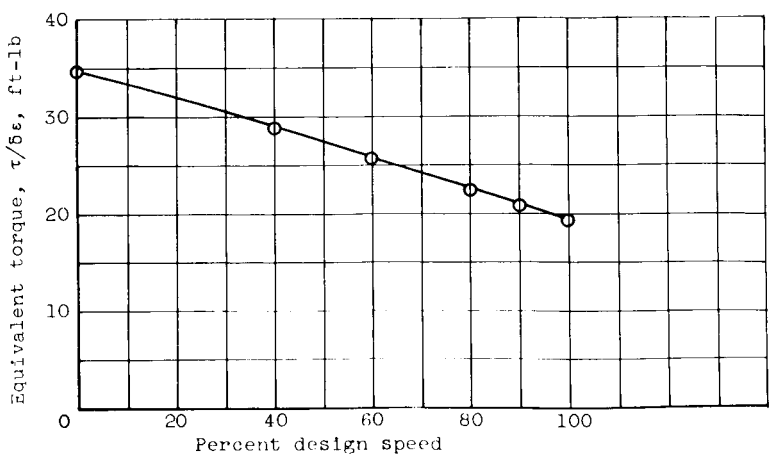


(c) Variation of equivalent torque with speed at design total- to static-pressure ratio.

Figure 9. - Experimentally obtained turbine performance characteristics.

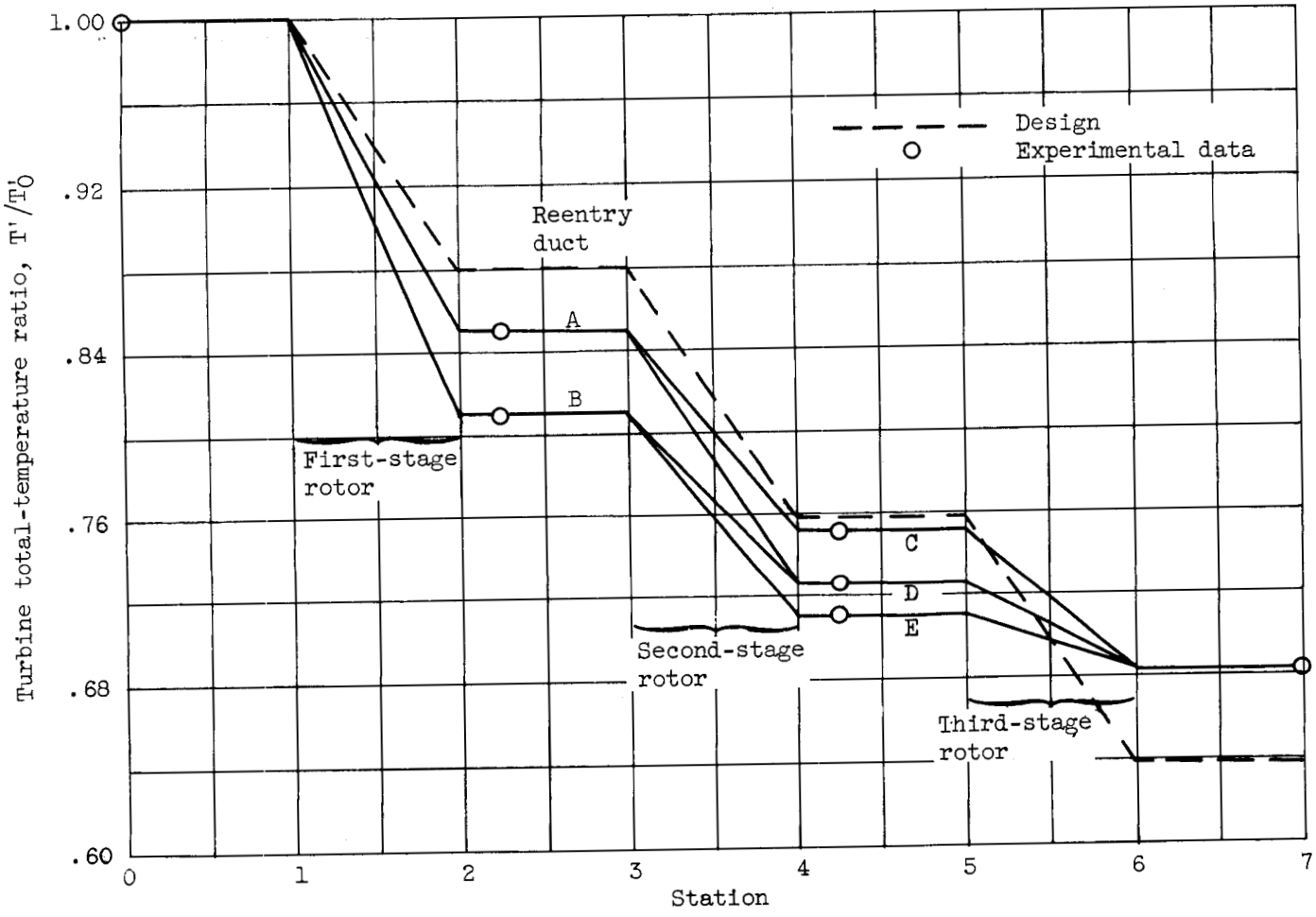


(a) Total-temperature variation inside turbine.

Figure 10. - Turbine over-all and interstage flow conditions at design speed and design total- to static-pressure ratio.

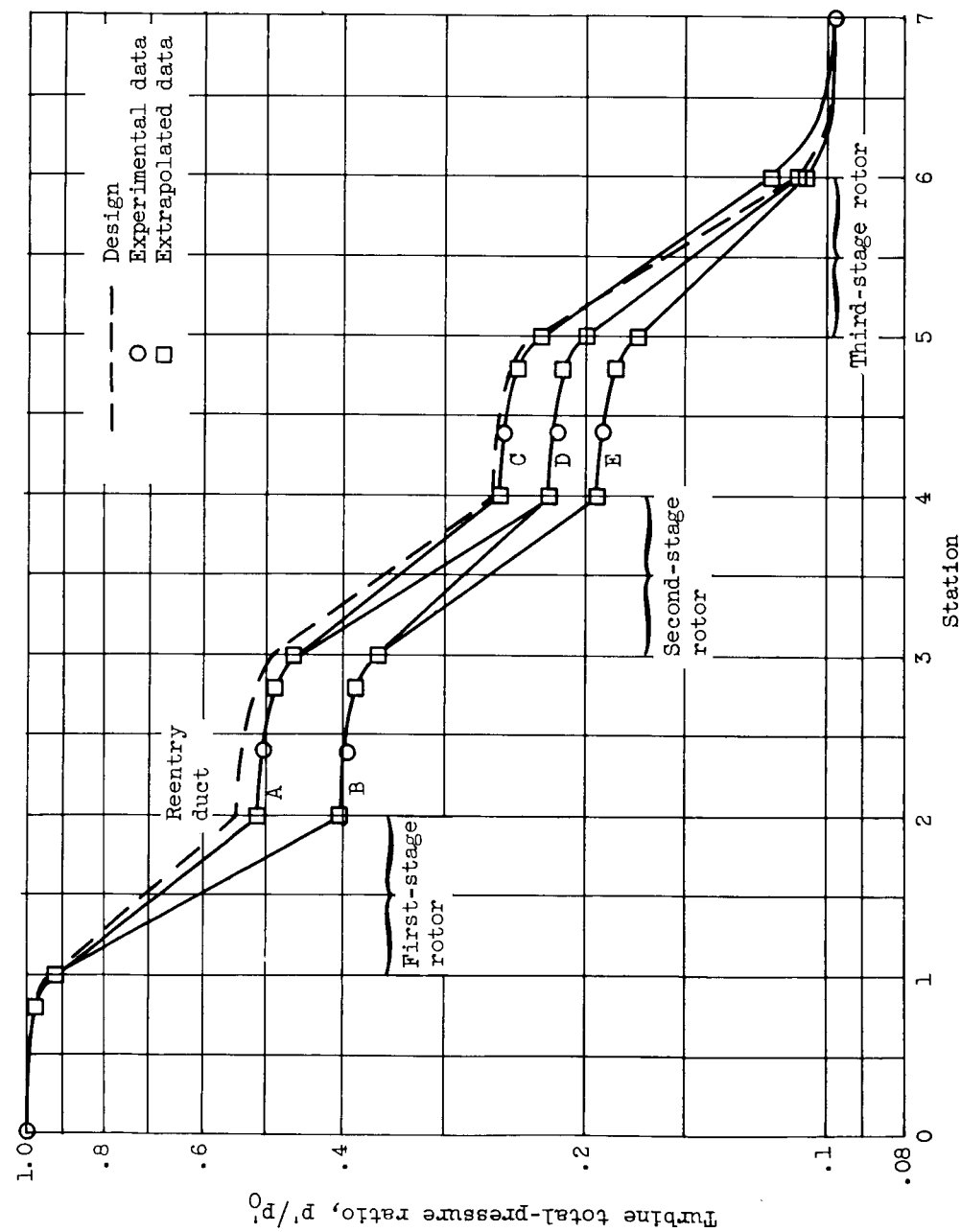


(b) Total-pressure variation inside turbine.

Figure 10. - Continued. Turbine over-all and interstage flow conditions at design speed and design total- to static-pressure ratio.

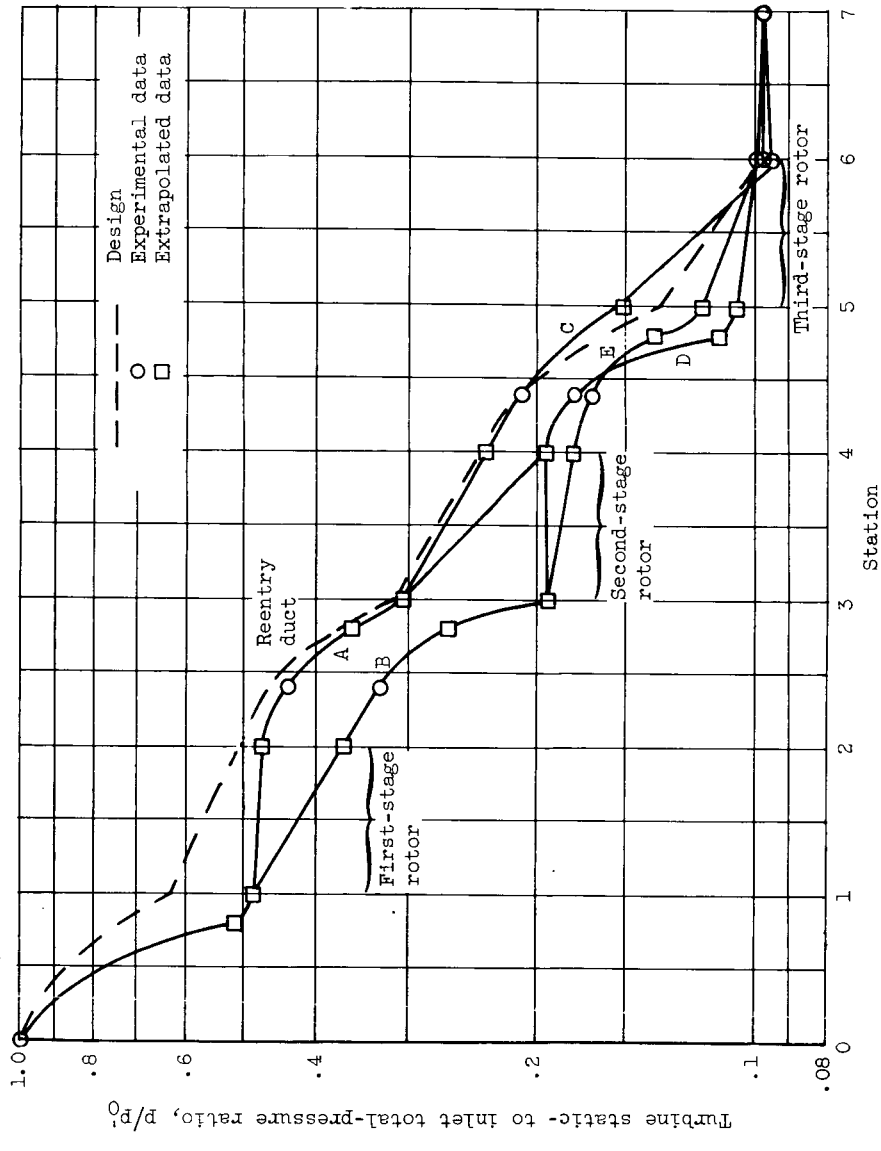


(c) Static-pressure variation inside turbine.

Figure 10. - Continued. Turbine over-all and interstage flow conditions at design speed and design total- to static-pressure ratio.

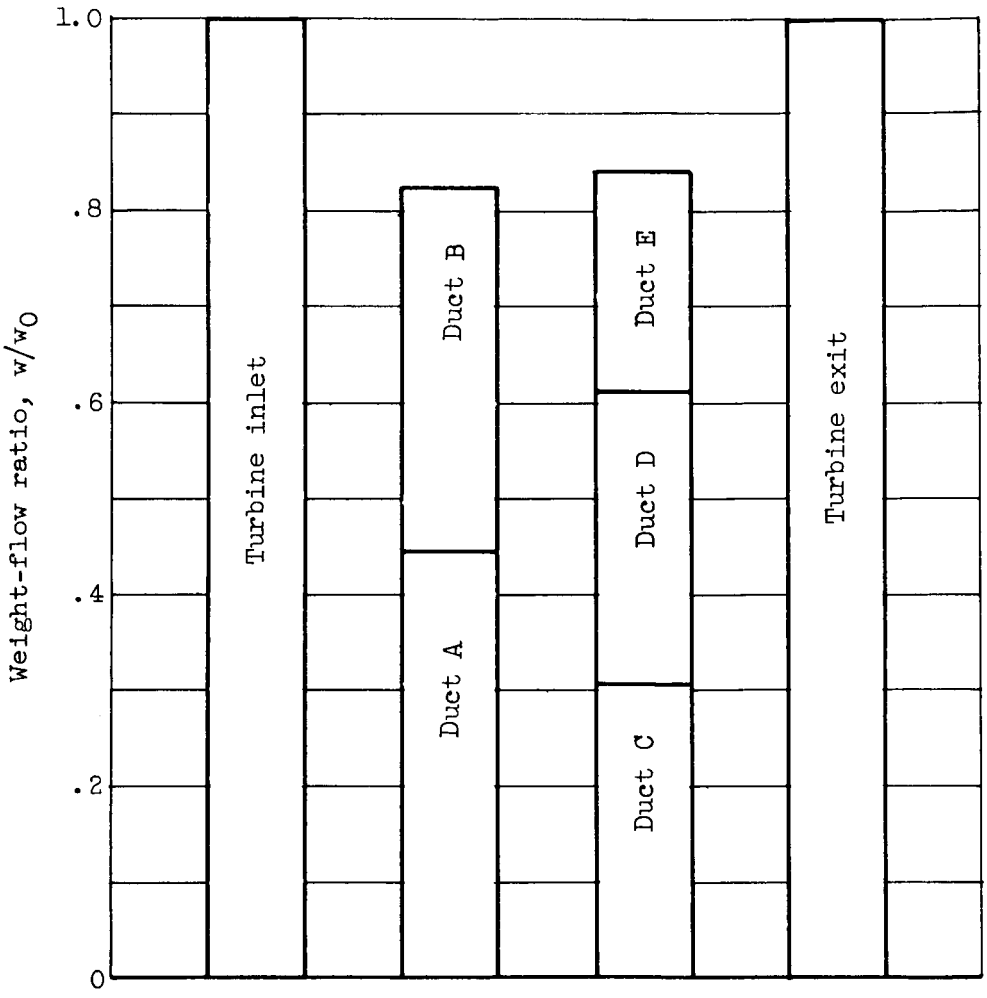


(d) Weight-flow variation inside turbine.

Figure 10. - Concluded. Turbine over-all and interstage flow conditions at design speed and design total- to static-pressure ratio.